Pergamon

Int. J. Heat Mass Transfer. Vol. 38, No. 12, pp. 2183–2193, 1995

0017-9310/95 $9.50+0.00

0017-9310(94)00345-9

An analysis of freeze-up phenomena during gas atomization of metals

H. LIU, E. J. LAVERNIA and R. H. RANGEL†

Department of Mechanical and Aerospace Engineering, University of California, Irvine, CA 92717, U.S.A.

(*Received* 18 *April* 1994 *and in final form* 26 *October* 1994)

Abstract—A numerical model is developed to describe the flow and heat transfer behavior of molten metals during flow in the delivery tube in gas atomization and spray deposition. Numerical simulations for Al, Cu, Mg, Ni, Ti and W melt are conducted to investigate the influence of processing parameters and material properties on the minimum melt superheat that is necessary to prevent the tube from premature solidification during delivery of the molten metal prior to atomization. Processing maps are developed to provide direct insight into the complex relationship among the minimum melt superheat, processing parameters and material properties. A quantitative correlation is obtained by means of a regression analysis of the numerical results, which facilitates application of the numerical model. The calculated results demonstrate that for the materials studied, the minimum melt superheat ranges from $0.005T_m$ to $0.19T_m$, depending on processing parameters and material properties. The dependence can be expressed using a correlation derived from the regression analysis such as

$$\frac{\Delta T}{T_m} = 0.15\left[\frac{\mu U^2}{kc_p\rho\Delta P}\frac{T_m}{T_g}\right]^{0.1}\left[\frac{L}{D}\right]^{0.3}.$$

Increasing the overpressure can effectively decrease the minimum melt superheat, especially for a large tube-length : diameter ratio and for materials possessing low densities. This effect diminishes with increasing overpressure. The minimum melt superheat can also be decreased by reducing the tube length : diameter ratio, by selecting a smooth delivery tube with low thermal conductivity and thick tube wall, and/or by enhancing the ambient gas temperature. Materials with high thermal conductivity, high thermal capacity and/or large density allow a small melt superheat to prevent the delivery tube from freeze-up, while materials with high melting temperature and/or high viscosity require a large melt superheat.

1. INTRODUCTION

Over the past decade, spray atomization and deposition has attracted considerable attention as a processing alternative for producing net or near-net shape materials [1]. A number of investigators have conducted numerical or experimental studies to elucidate fundamental mechanisms that govern the disintegration of liquid metals [2–4], size distribution of atomized droplets [5, 6], gas flow and rapid solidification of droplets [7–11], as well as the evolution of microstructure in droplets [12–14] during gas atomization. Inspection of the relevant literature, however, reveals that the freeze-up phenomenon of melt in the delivery tube during gas atomization has not been addressed properly in earlier studies. In gas atomization of liquid metals and alloys, freeze-up of melt in the delivery tube is an inherent problem which may occur when processing parameters are improperly selected. Therefore, the primary objective of the present study is to elucidate the inherent relationship between various processing parameters and the melt superheat that is necessary to prevent the delivery tube from freeze-up during gas atomization. Accordingly, a numerical model is developed on the basis of the boundary layer theory and the modified van Driest and Cebeci mixing length turbulence model to investigate the flow and heat transfer behavior of melt in the delivery tube. Numerical calculations are conducted for different metal and alloy systems to examine effects of thermal properties of the materials on the freeze-up phenomenon. On the basis of the numerical calculations, the concept of processing maps is introduced and a quantitative correlation is established in order to facilitate the application of the numerical model and results.

2. NUMERICAL MODEL

In gas atomization, liquid metals are generally transported from a melting crucible to the atomizer through a delivery tube, as schematically shown in Fig. 1(a). During flow through the delivery tube, the temperature of melt decreases gradually, primarily because of the heat exchange with the tube wall. Premature solidification of melt in the delivery tube (referred to hereafter as freeze-up) may occur when the melt temperature decreases down to or below the

† Author to whom correspondence should be addressed.

NOMENCLATURE

A_{cs} cross sectional area of delivery tube, $A_{cs} = \pi D^2/4$ [m^2]
A^+, B^+ momentum and thermal damping coefficients, respectively, $A^+ = 26$ [17]
c constant related to geometric progression of grid spacing, $c = 1.15$ [16]
c_0 discharge coefficient of melt, $c_0 = 0.82$ [28]
c_p thermal capacity of melt [J kg^{-1} K^{-1}]
C_i constants for calculation of thermal damping coefficient
D, L, D_w diameter and length of delivery tube, and thickness of tube wall, respectively, [m]
E viscous activation energy [J mol^{-1}]
g gravity acceleration [m s^{-2}]
H height of melt in melting crucible, $H = 0.16$ [23] [m]
j subscript denoting grid order
k, k_t, k_{eff}, k_w thermal conductivity, turbulent conductivity and effective conductivity of melt, and thermal conductivity of tube wall, respectively [W m^{-1} K^{-1}]
K, K' mixing-length constants of momentum and heat, respectively, $K = 0.435$[17], $K' = 0.44$[17]
l, l_t mixing-length for momentum and heat, respectively
$\dot{m}$ mass flow rate of melt [kg s^{-1}]
P, ΔP pressure and overpressure, respectively [Pa]
Pr Prandtl number, $Pr = c_p\mu/k$
r, x radial and axial coordinate, respectively [m]
R Radius of delivery tube [m]
$\mathfrak{R}$ constant in temperature equation of viscosity, $\mathfrak{R} = 8.314$ [J K^{-1} mol^{-1}]
T, T_0 melt temperature and its initial value, respectively [K]
T_m, T_g melting temperature of material and gas temperature, respectively [K]
ΔT melt superheat, $\Delta T = T_0 - T_m$ [K]
u, v, u_0 axial and radial velocity of melt, as well as initial axial velocity, respectively [m s^{-1}]
U, $U_{external}$ overall heat-transfer coefficient between melt at tube wall and ambience, and between outside of tube and ambience, respectively [W m^{-2} K^{-1}]
y, Δy distance from tube wall, $y = R - r$, and grid spacing in radial direction, respectively [m]
y^+ dimensionless distance from tube wall, $y^+ = y\sqrt{(\tau_w/\rho)}/(\mu/\rho)$.

Greek symbols
ρ, ρ_0 density of melt at arbitrary temperature and at melting point, respectively [kg m^{-3}], $\rho = \rho_0 - (d\rho/dT)(T - T_m)$
μ, μ_0, μ_t, μ_{eff} viscosity of melt at arbitrary temperature, viscosity constant, eddy viscosity and effective viscosity, respectively [N s m^{-2}], $\mu = \mu_0 \exp(E/\mathfrak{R}T)$
τ_w local wall shear stress [N m^{-2}].

melting temperature. The freeze-up is caused basically by: (a) inadequate melt superheat; (b) excessive residence time of melt in the delivery tube and (c) recirculation of undercooled droplets at the tube exit. The selection of an appropriate melt superheat requires that it can offset the heat loss of melt during the flow in the delivery tube. The heat loss and the residence time of melt are closely related to the flow and heat transfer behavior in the tube.

Under the conditions of practical interest, the flow of melt in the delivery tube is turbulent due to the very low kinematic viscosity that is inherent in most liquid metals. The Peclet number is typically larger than 50, so that the axial momentum and thermal diffusion is negligible compared to the radial ones. The axial velocities and length, however, are much larger than those in the radial direction. Hence, boundary layer approximations may be employed to formulate the problem of the flow and heat transfer in the tube, except in the region very near the entrance of the tube. In addition, the tube length : diameter ratio is typically smaller than 20. Therefore, the flow is not fully developed either hydrodynamically or thermally. With the assumptions of steady and axisymmetric flow, the governing equations for the flow and heat transfer of melt can be written in cylindrical coordinates (Fig. 1(b)) as

$$\frac{\partial(\rho u)}{\partial x} + \frac{1}{r}\frac{\partial(\rho v r)}{\partial r} = 0 \tag{1}$$

$$\rho u\frac{\partial u}{\partial x} + \rho v\frac{\partial u}{\partial r} = \rho g - \frac{dp}{dx} + \frac{1}{r}\frac{\partial}{\partial r}\left(\mu_{eff} r\frac{\partial u}{\partial r}\right) \tag{2}$$

$$\rho c_p\left(u\frac{\partial T}{\partial x} + v\frac{\partial T}{\partial r}\right) = u\frac{dp}{dx} + \frac{1}{r}\frac{\partial}{\partial r}\left(k_{eff} r\frac{\partial T}{\partial r}\right) + \mu_{eff}\left(\frac{\partial u}{\partial r}\right)^2 \tag{3}$$

$$\dot{m} = \int_{A_{cs}} \rho u\, dA_{cs} = \text{constant} \tag{4}$$

for continuity, momentum, energy and integral con-

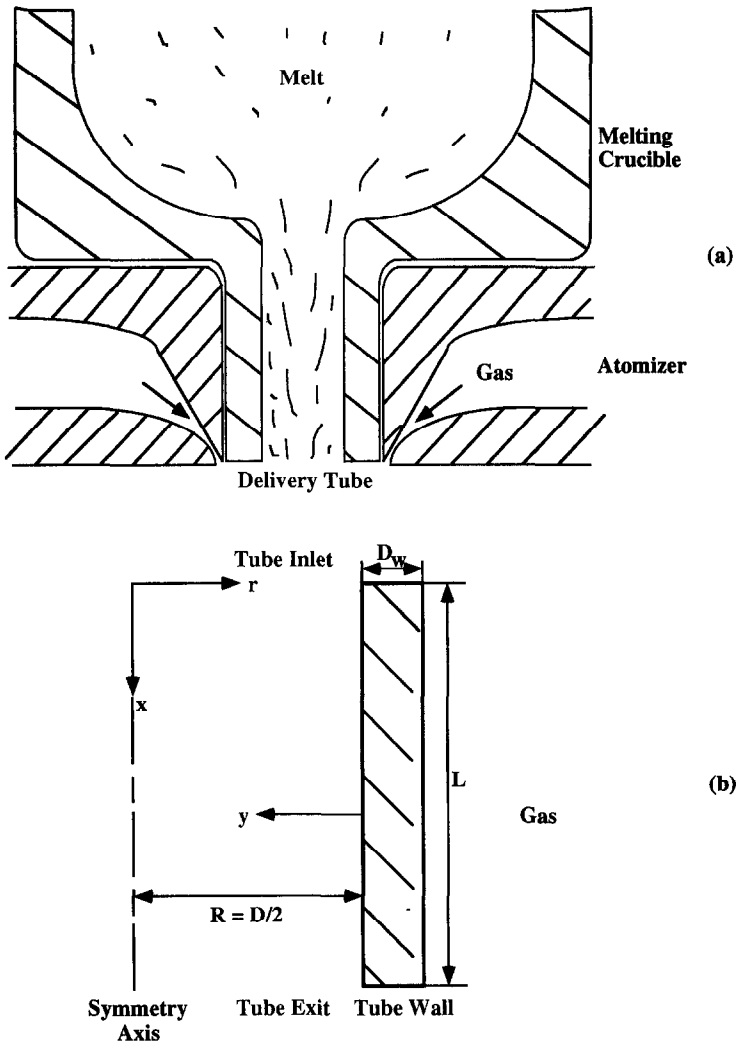

Fig. 1. Schematic diagram showing delivery tube and cylindrical coordinates used for numerical calculations of flow in tube.

tinuity, respectively. In the momentum equation and energy equation, the body force and the viscous dissipation are also included.

Some related studies [15–17] on turbulent flow and heat transfer in the entrance region of pipes have shown that the van Driest turbulence model [18] can produce very good agreement with experiments. The turbulent transport properties, therefore, are modeled using the eddy viscosity μ_t and the turbulent conductivity k_t on the basis of the van Driest [18] and Cebeci [19] mixing length turbulence models such that

$$\mu_{\text{eff}} = \mu + \mu_t = \mu + \rho l^2 \left|\frac{\partial u}{\partial y}\right| \tag{5}$$

$$k_{\text{eff}} = k + k_t = k + \rho l l_t c_p \left|\frac{\partial u}{\partial y}\right| \tag{6}$$

with

$$l = \begin{cases} Ky[1-\exp(-y^+/A^+)] & 0 < y \leqslant \dfrac{0.09R}{K} \\ 0.09R & y > \dfrac{0.09R}{K} \end{cases} \tag{7}$$

and

$$l_t = K'y[1-\exp(-y^+\sqrt{Pr}/B^+)]. \tag{8}$$

Here the mixing-length for heat, l_t, is employed according to the concept of turbulent Prandtl number [19] which provides a functional link between turbulent momentum transport and turbulent energy transport. This selection is prompted by the fact that liquid metals possess very low Prandtl number so that the Reynolds analogy is no longer valid. The mixing-length constants for momentum and heat as well as the damping coefficient for momentum are evaluated

according to Chen and Chiou [17]. The thermal damping coefficient is approximated using the extended form of the Cebeci model [19], as proposed by Na and Habib [20] for liquids of low Prandtl number

$$B^+ = \sum_{i=1}^{5} C_i(\log_{10} Pr)^{i-1} \tag{9}$$

with $C_1 = 34.96$, $C_2 = 28.79$, $C_3 = 33.95$, $C_4 = 6.33$ and $C_5 = -1.186$ [20].

At the inlet of the tube, uniform melt velocity and temperature are assumed

$$u(r,0) = u_0 \quad T(r,0) = T_0. \tag{10}$$

On the basis of Bernoulli's equation, the initial flow velocity of melt at the inlet of the tube may be calculated using the following formulation

$$u_0 = c_0\sqrt{\left[2g\left(H+\frac{\Delta P}{\rho g}\right)\right]}. \tag{11}$$

At the center line of the tube, the symmetry condition requires that

$$\frac{\partial u}{\partial r}(0,x) = 0 \quad v(0,x) = 0 \quad \frac{\partial T}{\partial r}(0,x) = 0. \tag{12}$$

The second of these cannot be satisfied by the boundary-layer equations and is imposed when solving the energy equation in order to satisfy the requirement of symmetry at the centerline. Since the temperature profile near the inlet is uniform in the core of the channel, the actual behavior of the radial velocity profile does not significantly affect the results.

At the tube wall

$$u(R,x) = 0 \quad v(R,x) = 0 \tag{13}$$

and an energy balance condition for temperatures are applied

$$-k\frac{\partial T}{\partial r}(R,x) = U(T(R,x) - T_g). \tag{14}$$

In the near wall region, the turbulent thermal conductivity is small compared to the extremely large molecular thermal conductivity of liquid metals, and hence can be neglected. T_g represents an ambient temperature which may be the temperature of atomization gas, and U is an overall heat-transfer coefficient which may include the heat conduction resistance of the tube wall and the heat-transfer resistance in the outside region of the tube (Fig. 1(b))

$$\frac{1}{U} = \frac{R}{k_w}\ln\left(1+\frac{D_w}{R}\right) + \frac{1}{U_{external}} \tag{15}$$

where the comprehensive heat-transfer coefficient $U_{external}$ reflects a total heat-transfer resistance in the external region of the tube which depends on external gas flow, atomizer geometry and atomizer–delivery tube configuration, and hence is apparatus-specific. In the practice of gas atomization of metals, however, this heat-transfer coefficient normally is significantly large due to high gas flow velocity, leading to a negligible contribution of the second term on the right hand side of equation (15) to the overall heat-transfer coefficient. Hence, the influence of the heat-transfer coefficient $U_{external}$ on the melt heat transfer is not addressed in the present study.

The governing equations along with the initial and boundary conditions described above are solved using an explicit, non-iterative finite-difference scheme of DuFort-Frankel type [16]. This method is applicable to simultaneous hydrodynamic and thermal entry conditions, i.e. developing thermal and velocity (DTV) region of pipe flow, and is faster than the implicit method of Patankar and Spalding [21] due to its non-iterative nature [16]. Since the details of the numerical procedure have been extensively described in [16], they will not be repeated herein. In the present study, 40 nodes in a radial direction are employed with geometric progression on grid spacing and the finest grid near the wall:

$$y(j) = \begin{cases} 0 & j = 1 \\ y(j-1) + \Delta y(j-1) & j = 2,40 \end{cases} \tag{16}$$

$$\Delta y(j) = \begin{cases} \dfrac{D}{2}\dfrac{(1-c)}{(1-c^{39})} & j = 1 \\ c\cdot\Delta y(j-1) & j = 2,39. \end{cases} \tag{17}$$

The forward marching step length ranging from $\Delta y(1)$ to $2\Delta y(1)$ is selected to satisfy the stability constraint and to obtain a good accuracy. To verify the numerical accuracy, several calculations are conducted with different grid spacing until grid independent results are obtained. Test calculations are also performed with some initial conditions for which reliable analytical and experimental results are available in order to verify the present numerical calculations. All calculations are performed on a DEC 5000/240 workstation.

3. RESULTS AND DISCUSSION

Numerical calculations are conducted for six representative materials: Al, Cu, Mg, Ni, Ti and W, encompassing a wide range of material properties, as summarized in Table 1. The processing parameters considered include melt superheat, ΔT, overpressure, ΔP, tube length, L, tube diameter, D, gas temperature, T_g and overall heat-transfer coefficient, U. A melt superheat up to a maximum of 450 K and an overpressure ranging from 0.006, 60 to 600 kPa are examined. The gas temperature is assumed to change from 200 to 300 K. A tube length of 20, 35 to 50 mm and a tube diameter of 3, 6 to 9 mm are considered. Overall heat-transfer coefficients of 4000 and 8000 $W\,m^{-2}\,K^{-1}$ are used in the calculations to simulate two cases which are common in the practice of gas atomization of metals. The velocity and temperature distributions of the liquid metals are calculated for each combination of the above conditions. For each given melt

Table 1. Physical properties of liquid metals investigated in the present study

Material	T_m [K]	k [W m^{-1} K^{-1}]	c_p [J kg^{-1} K^{-1}]	ρ_0 [kg m^{-3}]	$d\rho/dT$ [kg m^{-3} K^{-1}]	μ_0 [mN s m^{-2}]	E [kJ mol^{-1}]
Refs.	[24]	[25]	[24]	[27]	[27]	[27]	[27]
Al	933	100	1178	2385	0.280	0.149	16.500
Cu	1356	165	490	8000	0.801	0.301	30.500
Mg	923	90	1360	1590	0.265	0.025 [24]	30.500
Ni	1728	30	652	7905	1.160	0.166	50.200
Ti	1998	20 [26]	700 [26]	4110	0.702	0.321 [26]	46.279 [24]
W	3655	71 [26]	230 [26]	17600	1.500 [26]	0.129 [26]	95.528 [24]

superheat, the calculation is carried out until the melt temperature at the tube wall decreases to the melting temperature of the melt. The corresponding melt superheat is taken as the minimum superheat that is necessary to prevent the tube from freeze-up, referred to hereafter as minimum melt superheat.

3.1. *Melt velocity and temperature distributions in delivery tube*

The calculated velocity and temperature distributions of liquid Al during flow in the delivery tube are shown in Fig. 2. The velocity and temperature are normalized with their initial values, and the radial coordinate is normalized with the tube diameter. The results demonstrate that the melt velocity is not fully developed even in the region close to the exit of the tube (Fig. 2(a)). The radial velocity is smaller than 1% of the initial axial velocity at most axial locations, except for the region very close to the tube inlet (Fig. 2(b)). The higher radial velocities near the tube wall are typical in boundary layer development. The radial velocity, however, must go to zero at the center line due the symmetry condition ($v(0,x) = 0$ in equation (12)). This symmetry condition ensures that there is no convective heat flow across the center line. The overall velocity development is similar to that of ordinary fluids. In contrast, the thermal boundary layer develops quite fast and approaches a parabolic-type distribution at the axial distance close to the exit of the tube. This temperature distribution suggests that the molecular heat transport is significant, not only in the viscous sublayer, but also in the buffer zone and even in some part of the turbulent-core region. The molecular thermal diffusion can penetrate from the tube wall deep into the turbulent core. Such heat transfer characteristic is a direct consequence of the low values of the Prandtl numbers of liquid metals. Therefore, the magnitude of the Prandtl numbers has an important impact on the temperature distribution which, as will be discussed below, will eventually influence the minimum melt superheat.

3.2. *Effects of processing parameters on minimum melt superheat*

Figures 3–8 show the calculated minimum melt superheat for Al, Cu, Mg, Ni, Ti and W as a function of the overpressure. Also shown are the effects of the melting temperature of the metals, the gas temperature, the delivery tube length, and the delivery tube diameter on the minimum melt superheat. The overall heat-transfer coefficient is 8000 W m^{-2} K^{-1} for the results shown in these figures. It can be seen that the group of curves in each figure divide the graph into two primary zones. In the zone below a curve, freeze-up occurs regardless of the magnitude of the overpressure. In the zone above a curve, freeze-up will not take place. Overall, the minimum melt superheat ranges from 5 to 435 K, corresponding to dimensionless values $\Delta T/T_m$ from 0.005 to 0.19, depending on processing parameters and material properties. On the basis of the information summarized in these figures, it is possible to select the processing conditions that are necessary to avoid freeze-up. Hence, the figures are referred to hereafter as 'processing maps'.

The processing maps for the different materials reveal some common trends. First, within the range of low overpressure values (for example, $\Delta P \leqslant 60$ kPa), increasing the overpressure can effectively decrease the minimum melt superheat, especially for a large tube-length : diameter ratio (for example, $L : D = 17$) and for materials of low densities (for example, Al and Mg). This effect diminishes with increasing overpressure. Second, for a constant value of the overpressure, the minimum melt superheat decreases with decreasing tube-length : diameter ratio or decreasing melting-temperature : gas-temperature ratio. Similarly, for a constant value of the melt superheat, the overpressure, which is necessary to avoid freeze-up (referred to hereafter as minimum overpressure), decreases with decreasing tube-length : diameter ratio or decreasing melting-temperature : gas-temperature ratio.

These results are not unexpected. Indeed, increasing overpressure can increase the flow velocity of melt and decrease the residence time of melt in the tube, hence reducing the heat loss from melt to tube. This effect dominates the heat transfer behavior of melt within the range of the low overpressure values. Therefore, increasing the overpressure leads to a significant decrease in the minimum melt superheat. On the other hand, a further increase in overpressure leads to an increase in the average cooling rate of melt as a result of the increased flow velocity of melt. Hence, the heat loss from the melt to the tube can not be significantly

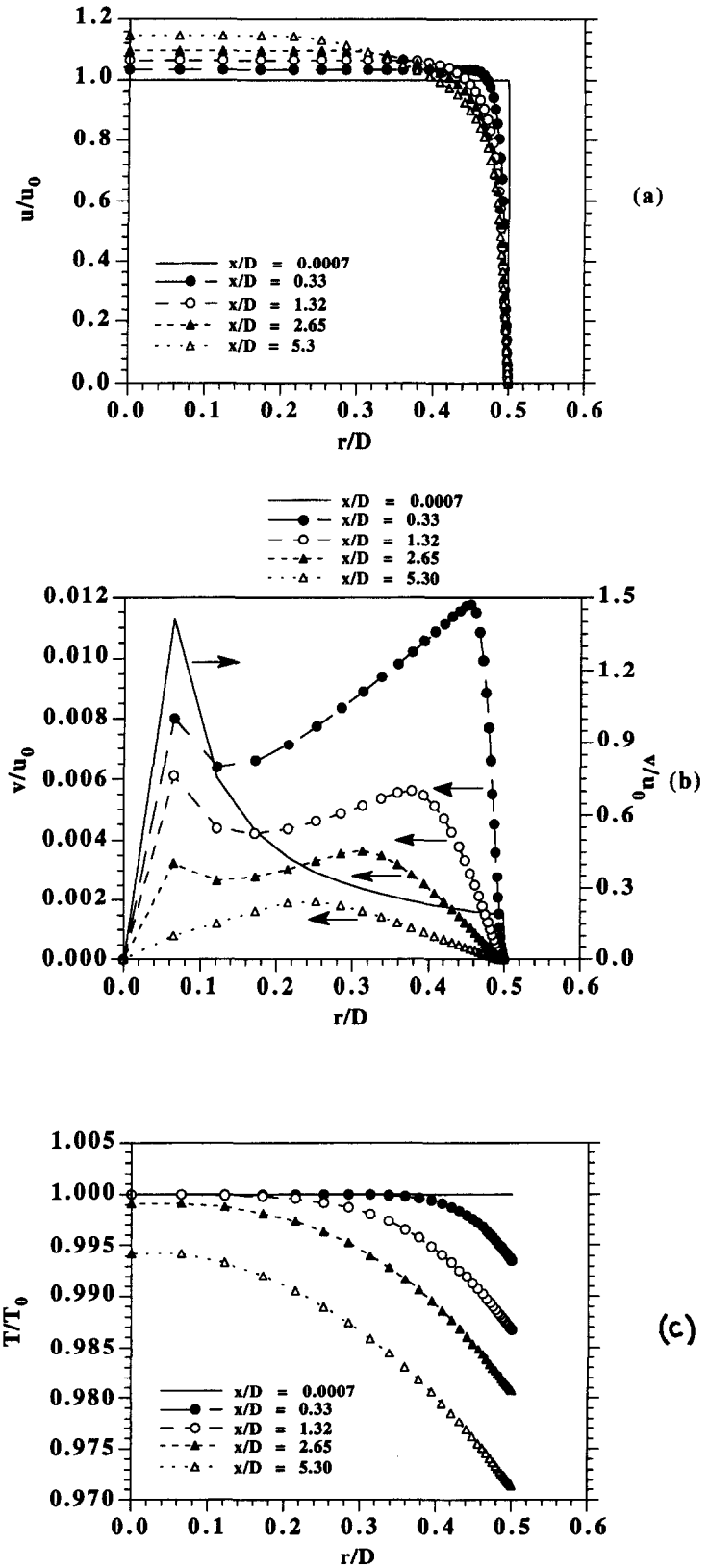

Fig. 2. Melt velocity and temperature profiles in DTV region of delivery tube: (a) axial velocity; (b) radial velocity and (c) temperature.

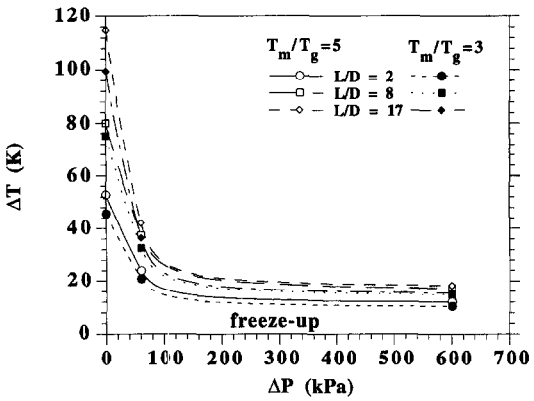

Fig. 3. Effect of processing parameters on minimum melt superheat for Al (U = 8000 W m^{-2} K^{-1}).

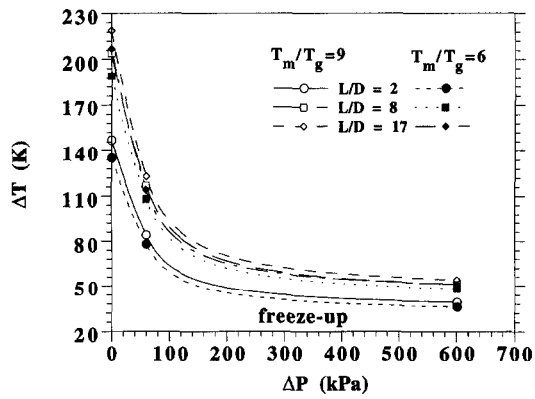

Fig. 6. Effect of processing parameters on minimum melt superheat for Ni (U = 8000 W m^{-2} K^{-1}).

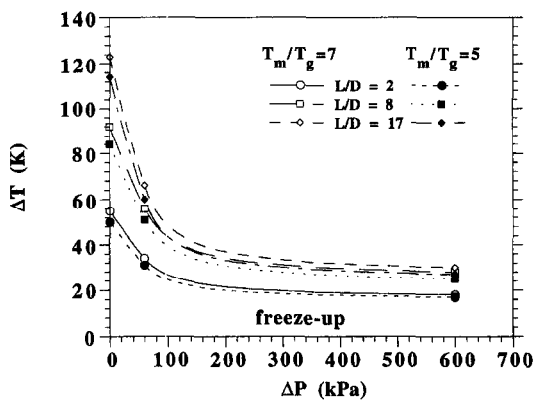

Fig. 4. Effect of processing parameters on minimum melt superheat for Cu (U = 8000 W m^{-2} K^{-1}).

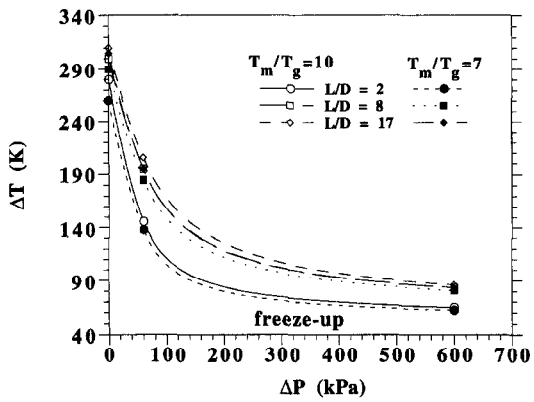

Fig. 7. Effect of processing parameters on minimum melt superheat for Ti (U = 8000 W m^{-2} K^{-1}).

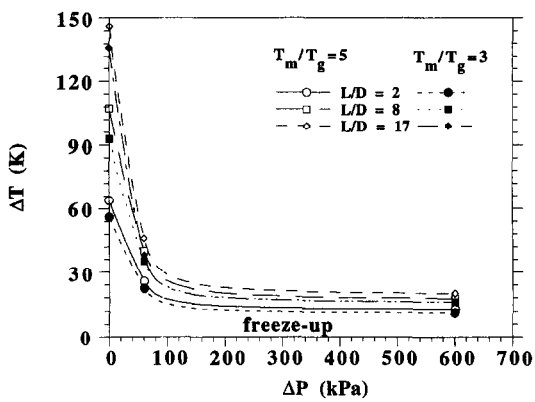

Fig. 5. Effect of processing parameters on minimum melt superheat for Mg (U = 8000 W m^{-2} K^{-1}).

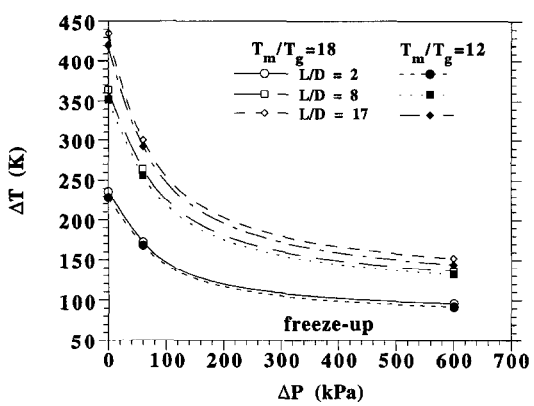

Fig. 8. Effect of processing parameters on minimum melt superheat for W (U = 8000 W m^{-2} K^{-1}).

reduced further. This effect becomes increasingly important within the range of the high overpressure values. Thus, further increasing overpressure can not reduce the minimum melt superheat significantly.

The effects of the tube length, tube diameter, melting temperature and gas temperature on the minimum melt superheat are relatively straightforward. Increasing the tube length is equivalent to increasing the residence time of melt in the tube, while decreasing the tube diameter or increasing the melting-temperature : gas-temperature ratio increases the average cooling experienced by the melt. Therefore, a large tube-length : diameter ratio or melting-temperature : gas-temperature ratio requires a large minimum melt superheat.

The influence of the physical properties of melt on

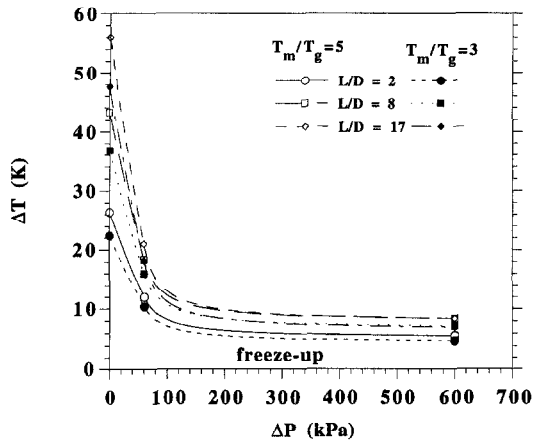

Fig. 9. Effect of processing parameters on minimum melt superheat for Al ($U = 4000$ W m^{-2} K^{-1}).

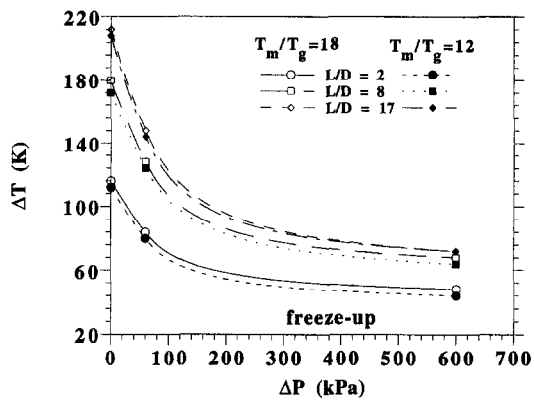

Fig. 11. Effect of processing parameters on minimum melt superheat for W ($U = 4000$ W m^{-2} K^{-1}).

the minimum melt superheat is also evident from the processing maps. Comparing the maps for Al, Cu, Mg, Ni, Ti and W melts, it can be seen that the minimum melt superheat is basically proportional to the melting temperature, i.e. increasing from Al, Cu, Ni, Ti to W, with an exception provided by Mg. This exception is attributable to the Prandtl number of molten Mg. The melting temperature and density of Mg are the lowest among the materials considered. However, the Prandtl number of molten Mg is larger than those of molten Al and Cu. This is the reason why the minimum melt superheat for Mg is apparently higher at the small overpressure values relative to those for Al and Cu. However, at the large overpressure values, the minimum melt superheat for Mg becomes low due to the sensitivity of its flow velocity to overpressure.

Figures 9–11 show the calculated minimum melt superheat for Al, Cu and W as a function of the overpressure. The overall heat-transfer coefficient is 4000 W m^{-2} K^{-1} for the results shown in these figures. Comparing these figures to Figs. 3, 4 and 8 (where the overall heat-transfer coefficient is 8000 W m^{-2} K^{-1}), the influence of the tube wall heat-transfer characteristics on the minimum melt superheat can be deduced. Clearly, the minimum melt superheat is reduced significantly when the overall heat-transfer coefficient decreases from 8000 to 4000 W m^{-2} K^{-1}, especially at the low overpressure values. This is a direct consequence of the reduced heat loss from melt to tube at the low heat-transfer coefficient. The overall heat-transfer coefficient is proportional to the thermal conductivity of the tube wall material and inversely proportional to the thickness of the tube wall. Hence, these results suggest that selecting a delivery tube with a good thermal isolation (low thermal conductivity) and a thick tube wall allows a low minimum melt superheat.

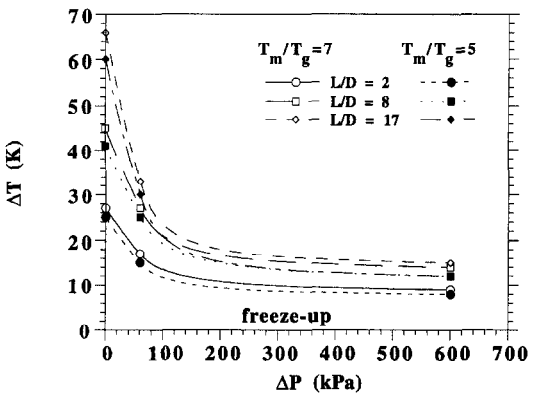

Fig. 10. Effect of processing parameters on minimum melt superheat for Cu ($U = 4000$ W m^{-2} K^{-1}).

3.3. *Correlation between processing parameters and minimum melt superheat*

The results discussed above demonstrate that the overpressure, delivery tube length and diameter, gas temperature, tube wall heat-transfer characteristics and material properties are the important factors which affect the minimum melt superheat. In order to provide direct insight into the complex relationship between these factors and to facilitate application of the model and results, a regression analysis of the numerical results is conducted and a quantitative correlation of the following form is derived from the analysis:

$$\frac{\Delta T}{T_m} = 0.15\left[\frac{\mu U^2}{k c_p \rho \Delta P}\frac{T_m}{T_g}\right]^{0.1}\left[\frac{L}{D}\right]^{0.3} \tag{18}$$

where the material properties are evaluated at the melting temperature. The left hand side of the correlation is the dimensionless minimum melt superheat. The right hand side of the correlation represents a combination of the Prandtl number, Euler number, Reynolds number and Nusselt number, as well as temperature and length ratios T_m/T_g and L/D, and hence is dimensionless. The selection of the relevant dimensional variables is based on the numerical simulation described above and our experimental observations, and the independent dimensionless variables are

chosen by applying the generally accepted dimensional analysis technique, i.e. the Buckingham Pi Theorem, to the present system. Equation (18) is accurate within 10%.

It is evident from this correlation that the minimum melt superheat can be decreased by reducing the tube length: diameter ratio, reducing the overall heat-transfer coefficient (selecting tube with low thermal conductivity and thick tube wall), imposing a high overpressure, or enhancing gas temperature. Materials possessing high thermal conductivity, high thermal capacity and/or large density allow a small minimum melt superheat, whereas materials possessing high melting temperature and/or high viscosity require a large minimum melt superheat.

From the results presented so far it can be noted that surface tension effects have not been considered in the present study. Surface tension typically affects the wetting behavior of melt with the tube wall. As revealed by an extensive amount of experimental investigation on the effects of wetting on liquid metal heat transfer [22], wetting or lack of wetting, of itself, does not significantly affect the heat transfer from liquid metals to tube. However, a non-wetting solid–liquid surface may suffer more readily from gas entrainment problems and impurities and particles may more easily become trapped, with concomitant decrease in heat transfer from melt to tube. Therefore, it can be expected that for materials with a high surface tension, the minimum melt superheat calculated here represents an upper bound. Moreover, the surface roughness of the delivery tube has not been considered in the present calculations. The surface roughness of the delivery tube typically influences the flow and heat transfer behavior. Experimental observations reveal that the convective heat-transfer coefficient between a fluid and a rough-surfaced tube is about 15–25% higher than that between the fluid and a smooth-surfaced tube under the same flow conditions [28]. Therefore, it is important to select a delivery tube with smooth surface for reducing the minimum melt superheat. In addition, considering the effects of the surface roughness, the pre-basal coefficient in the regression expression for the minimum melt superheat (equation (18)) has been increased by 25% in order to predict a safe estimate of the minimum melt superheat.

Finally, it should be emphasized that the minimum melt superheat calculated here is only a necessary condition, not a *sufficient* condition. In fact, our earlier experiments demonstrate that freeze-up may occur even for melt superheats that are higher than those calculated, if recirculating vortices form in the exit region of the delivery tube [23]. As schematically shown in Fig. 12, the recirculating gas flow in this region drags relatively cool or undercooled droplets upwards, and deposits them on the tip of the delivery tube, where they eventually solidify. The solidified metal continues to increase in thickness during atomization, eventually choking the flow of melt, a phenomenon that has been previously described as freeze-up. Therefore, it is necessary to design the geometry of the atomizer and select the position of the delivery tube in such a way as to minimize the presence of the recirculating gas flow in this region. A sufficient condition to avoid freeze-up must be determined by examining the flow field below the delivery tube. However, if the geometry and configuration of the delivery tube and the atomization gas nozzles are arranged in such a way that the recirculating vortex velocity is not large enough to drag cool droplets up to the delivery tube tip, then employing the melt superheat predicted herein may avoid freeze-up.

4. CONCLUSIONS

A numerical model is developed to describe the flow and heat transfer behavior of molten metals during flow in the delivery tube in gas atomization and spray deposition. Numerical simulations for Al, Cu, Mg, Ni, Ti and W melt are conducted to investigate the influence of processing parameters and material properties on the minimum melt superheat that is necessary to prevent the tube from premature solidification during delivery of the molten metal prior to atomization. Processing maps are developed to provide direct insight into the complex relationship among the minimum melt superheat, processing parameters and material properties. A quantitative correlation is obtained by means of a regression analysis of the numerical results, which facilitates application of the numerical model. From the numerical results, some primary concluding remarks may be summarized as follows:

(1) For the materials studied, the minimum melt superheat ranges from $0.005T_m$ to $0.19T_m$, depending on processing parameters and material properties. The dependence can be expressed using the following correlation derived from the regression analysis of the numerical results

$$\frac{\Delta T}{T_m} = 0.15\left[\frac{\mu U^2}{kc_p\rho\Delta P}\frac{T_m}{T_g}\right]^{0.1}\left[\frac{L}{D}\right]^{0.3}.$$

(2) Within the range of low overpressure values (for example, $\Delta P \leqslant 60$ kPa), increasing the overpressure can effectively decrease the minimum melt superheat, especially for a large tube-length: diameter ratio (for example, $L/D = 17$) and for materials of low densities (for example, Al and Mg). This effect diminishes with further increase in overpressure.

(3) The minimum melt superheat can be decreased by reducing the tube length: diameter ratio, by selecting a smooth delivery tube with low thermal conductivity and thick tube wall, and/or by enhancing the ambient gas temperature.

(4) Materials with high thermal conductivity, high thermal capacity and/or large density allow a small minimum melt superheat, whereas materials with high melting temperature and/or high viscosity require a large minimum melt superheat.

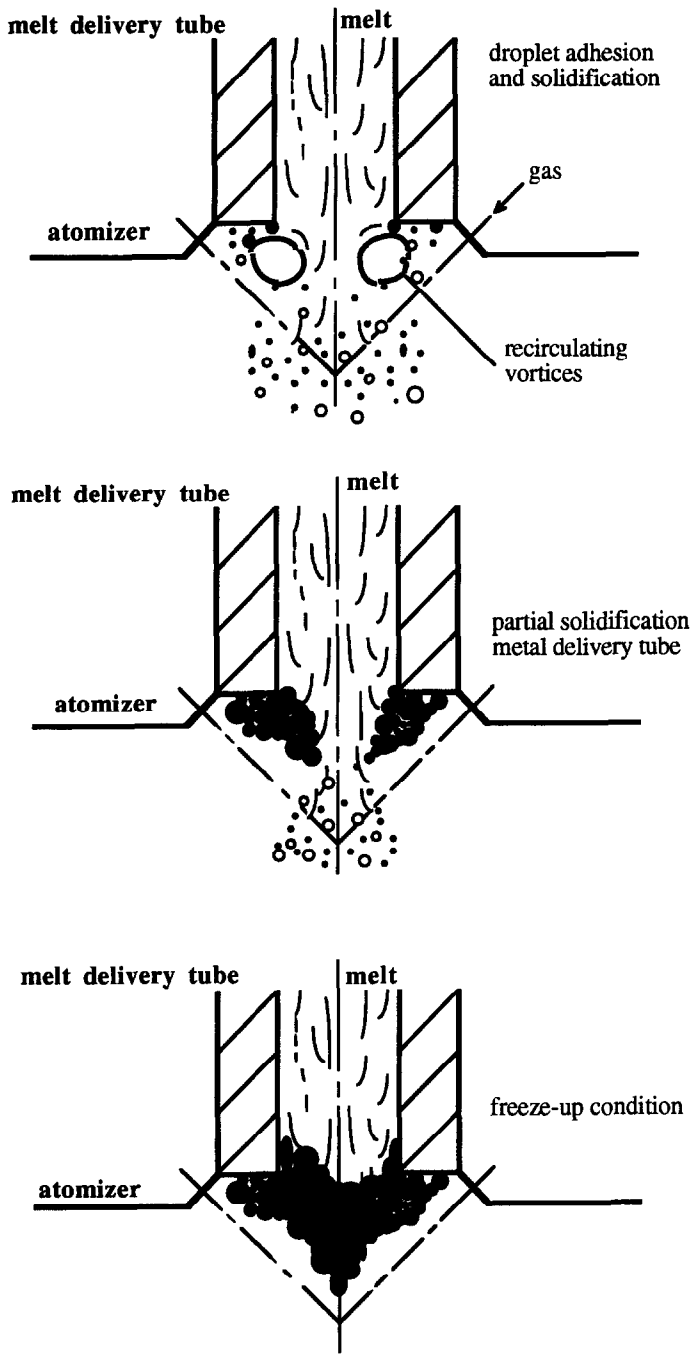

Fig. 12. Schematic diagram showing freeze-up phenomenon as a result of the presence of recirculating vortices.

(5) In order to minimize the probability of freeze-up, it is necessary to design the geometry of the atomizer and select the position of the delivery tube in such a way as to reduce the formation of recirculating gas flow in the region below the delivery tube.

Acknowledgements—The authors wish to acknowledge the Army Research Office (Grant DAALO3-92-G-0181) and the National Science Foundation (Grant CTS-9224850) for financial support. This research was also supported in part by the University of California, Irvine through an allocation of computer resources.

REFERENCES

1. E. J. Lavernia, J. D. Ayers and T. S. Srivatsan, Rapid solidification processing with specific application to aluminum alloys, *Int. Mater. Rev.* **37**, 1–44 (1992).
2. N. A. Chigier, The physics of atomization, *Proceedings of ICLASS*-91, National Institute of Standards and

Technology, U.S. Dept. of Commerce, pp. 1–15. 15–18 July (1991).
3. E. J. Lavernia, T. S. Srivatsan and R. H. Rangel, Atomization of alloy powders, *Atom. Sprays* **2,** 253–274 (1992).
4. J. B. See and G. H. Johnston, Interactions between nitrogen jets and liquid lead and tin stream, *Powder Technol.* **21,** 119–133 (1978).
5. H. Lubanska, Correlation of spray ring data for gas atomization of liquid metals, *J. Metals* **22,** 45–49 (1970).
6. S. L. Shinde and G. S. Tenkoldar, Analyses of atomization: a review, *Powder Metall. Int.* **9,** 180–184 (1977).
7. B. P. Bewlay and B. Cantor, Gas velocity measurements from a close-coupled spray deposition atomizer, *Mater. Sci. Engng A* **118,** 207–222 (1989).
8. E. J. Lavernia, E. M. Gutierrez, J. Szekely and N. J. Grant, A mathematical model of the liquid dynamic compaction process—I. Heat flow in gas atomization, *Int. J. Rapid Solidification* **4,** 89–124 (1988).
9. S. Annavarapu, D. Apelian and A. Lawley, Spray casting of steel strip—process analysis, *Metall. Trans. A* **21,** 3237–3256 (1990).
10. B. P. Bewlay and B. Cantor, Modeling of spray deposition: measurements of particle size, gas velocity, particle velocity, and spray temperature in gas-atomized sprays, *Metall. Trans. B* **21,** 899–912 (1990).
11. C. G. Levi and R. Mehrabian, Heat flow during rapid solidification of undercooled metal droplets, *Metall. Trans. A* **13,** 221–234 (1982).
12. X. Liang and E. J. Lavernia, Solidification and microstructure evolution during spray atomization and deposition of Ni_3Al, *Mater. Sci. Engng A* **161,** 221–235 (1993).
13. P. Mathur, D. Apelian and A. Lawley, Analysis of the spray deposition process, *Acta Metall.* **37,** 429–443 (1989).
14. E. Gutierrez-Miravete, E. J. Lavernia, G. M. Trapaga, J. Szekely and N. J. Grant, A mathematical model of the spray deposition process, *Metall. Trans. A* **20,** 71–85 (1989).
15. C. A. Bankston and D. M. McEligot, Turbulent and laminar heat transfer to gases with varying properties in the entry region of circular ducts, *Int. J. Heat Mass Transfer* **13,** 319–344 (1970).
16. R. M. Nelson and R. H. Pletcher, An explicit scheme for the calculation of confined turbulent flows with heat transfer, in *Proceedings of the* 1974 *Heat Transfer and Fluid Mechanics Institute*, Stanford University Press, Stanford, California, pp. 154–170.
17. C. J. Chen and J. S. Chiou, Laminar and turbulent heat transfer in the pipe entrance region for liquid metals, *Int. J. Heat Mass Transfer* **24,** 1179–1189 (1981).
18. E. R. Van Driest, On turbulent flow near a wall, *J. Aero. Sci.* **23,** 1007–1011 and 1036 (1956).
19. T. Cebeci, A model for eddy conductivity and turbulent Prandtl number, *J. Heat Transfer* **C95,** 227–234 (1973).
20. T. Y. Na and I. S. Habib, Heat transfer in turbulent pipe flow based on a new mixing length model, *J. Appl. Sci. Res.* **28,** 302–314 (1973).
21. S. V. Patankar and D. B. Spalding, *Heat and Mass Transfer in Boundary Layers* (2nd Edn). International Textbook, New York (1970).
22. S. Kakac, R. K. Shah and W. Aung, *Handbook of Single-Phase Convective Heat Transfer*. John Wiley, New York (1987).
23. X. Zeng, H. Liu, M. Chu and E. J. Lavernia, An experimental investigation of reactive atomization and deposition processing of Ni_3Al/Y_2O_3 using N_2–O_2 atomization, *Metall. Trans. A* **23,** 3394–3399 (1992).
24. T. Iida and R. I. L. Guthrie, *The Physical Properties of Liquid Metals*. Clarendon Press, Oxford (1988).
25. T. W. Clyne, Numerical treatment of rapid solidification, *Metall. Trans. B*, **15,** 369–381 (1984).
26. C. San Marchi, H. Liu, A. Sickinger, E. Mühlberger, E. J. Lavernia and R. H. Rangel, Numerical analysis of the deformation and solidification of a single droplet impinging onto a flat substrate, *J. Mater. Sci.* **28,** 3313–3321 (1993).
27. E. A. Brandes, *Smithell's Metals Reference Book* (6th Edn). Butterworths, London (1983).
28. D. Liu, *Fundamentals of Thermal Energy Engineering*. Metallurgy Industry Press, Beijing (1980).